



1
2
3
4
5
6
7
8
9
10
11
12
13
14
15
16
17
18
19
20
21
22
23
24
25
26
27
28
29
30
31

North Atlantic sea level budget revisited

Zhe Song^{1,2}, Anny Cazenave¹, William Llovel², Andrea Storto³ and Marie Bouih⁴

¹Université de Toulouse, LEGOS (CNES/CNRS/IRD/UT3), 31401 Toulouse, CEDEX 9, France

²Université de Bretagne Occidentale, CNRS, Ifremer, IRD, Laboratoire d'Océanographie Physique et Spatiale (LOPS), IUEM, 29280, Plouzané, France

³Institute of Marine Science, National Research Council of Italy, Rome, Italy

⁴Magellium, 31520 Ramonville St Agne, France

Correspondence to: Zhe Song (zhe.song@univ-brest.fr) and Anny Cazenave (anny.cazenave@univ-tlse3.fr, anny.cazenave@gmail.com)

Submitted to Ocean Science

February 2026



32 **Abstract**

33 Based on satellite altimetry, GRACE space gravimetry and Argo-based steric data down to
34 2000m, recent studies have shown that the North Atlantic sea level budget (i.e., altimetry-based
35 sea level minus sum of components) of the past two decades is not closed, with strong regional
36 residuals in the North Atlantic. This was suggested to result from salinity errors reported since
37 ~2015 in some Argo float measurements. In this study, we revisit the North Atlantic sea level
38 budget, using satellite altimetry, GRACE and GRACE-FO data, different Argo products and
39 two ocean reanalyses (CIGAR and ORAS5) over the 2004-2022 time span. The ocean
40 reanalyses are used to estimate the manometric contribution, an alternative to using GRACE
41 data, as well as the deep ocean contribution to the sea level budget, not yet fully sampled by
42 Argo. Analyzing different data sets allows us to evaluate their impact on the previously
43 reported non-closure of the North Atlantic sea level budget. We first find that using the CIGAR
44 ocean reanalysis-based manometric component significantly reduces the residuals of the North
45 Atlantic sea level budget compared to GRACE. We also find that accounting for the deep ocean
46 (below 2000m) thermal expansion (using the CIGAR reanalysis) allows for 30% reduction of
47 the North Atlantic budget residuals when using GRACE for the manometric component, while
48 the mean residual trend is reduced by a factor of 2 when using CIGAR for the manometric sea
49 level. In the latter case, the budget is closed within data uncertainties. The North Atlantic
50 halosteric component based on Argo and CIGAR in the upper 2000m displays a small decrease
51 since the early 2010s. However, this negative trend becomes stronger after 2016. The 2010–
52 2016 halosteric decrease may reflect a real salinity increase in the region, although salinity
53 measurement errors may have impacted the halosteric component after that date.

54



55 **1 Introduction**

56 While many studies have been devoted to assessing the global mean sea level budget over the
57 satellite altimetry era (1993 to present) (e.g., Barnoud et al., 2021; Bouih et al., 2025; Chen et
58 al., 2020; Dieng et al., 2017; Horwath et al., 2022; Llovel et al., 2023; Nerem et al., 2018;
59 WCRP, 2018) , only a few have focused on the regional sea level budget, with mixed results
60 (e.g., Bouih et al., 2025; Camargo et al., 2023; Frederikse et al., 2016; Hamlington et al., 2020;
61 Mu et al., 2024; Royston et al., 2020). At the global scale, the main terms of the sea level budget
62 are the global mean sea level rise and ocean mass (known as barystatic sea level, Gregory et
63 al., 2019) and thermosteric chang. At regional scale, however, other factors play a non-
64 negligible role, such as the halosteric (i.e., salinity-related) component, which makes the
65 regional sea level budget more complex to assess. In effect, a spurious salinity drift (giving rise
66 to an important halosteric component decrease) has been reported recently in some Argo-based
67 measurements (Liu et al., 2020; Ponte et al., 2021; Wong et al., 2023), that is supposed to have
68 a strong impact on the closure assessment of the regional sea level budget. Considering all
69 ocean basins, a recent study (Bouih et al., 2025) investigated the regional sea level trend budget
70 closure over the 2004-2022 time span, using altimetry-based sea level data, GRACE space
71 gravimetry for the regional ocean mass variations (also called manometric component, Gregory
72 et al., 2019) and Argo data for the steric (sum of thermosteric and halosteric terms) component
73 down to 2000m (global mean trends removed from all data sets). Bouih et al. (2025) also
74 considered several ocean reanalyses to compute the manometric component (an alternative to
75 using GRACE data), following the approach developed by Camargo et al. (2023), i.e., using
76 the sterodynamic sea level (Gregory et al., 2019) computed by the reanalysis and correcting it
77 for the local steric effect. The Bouih et al. (2025)'s study showed that in the Pacific, Indian and
78 South Atlantic Oceans, the sea level budget trend residuals (altimetry-based sea level minus
79 sum of components) were non-significant, considering the data uncertainties. On the other hand,
80 strong positive residuals were found in the North Atlantic, whatever the manometric



81 component considered (i.e., either from GRACE or from the ocean reanalyses). These authors
82 suspected the Argo-based spurious halosteric component (impacted by the Argo-based salinity
83 drift) as the cause of the non-closure of the sea level budget in the North Atlantic.

84 In the present study we revisit the question of the North Atlantic sea level budget over the
85 2004-2022 time span, using a variety of different data sets for the components of the sea level
86 budget: different GRACE mascon solutions and different Argo-based gridded products down
87 to 2000m, as well as two ocean reanalyses that provide an estimate of the steric signal from the
88 deep ocean. Our objective is to evaluate the impact of each product on the currently reported
89 non-closure of the North Atlantic sea level budget. An important addition compared to the
90 Bouih et al. (2025)'s study, indeed consists of accounting for the deep ocean warming below
91 2000m (not sampled by Argo) using estimates from the ocean reanalyses. This paper is
92 organized as follows. Section 2 presents the data and analysis method. Section 3 displays the
93 results for the North Atlantic sea level budget, both in terms of trend maps and time series. The
94 sea level budget excluding the North Atlantic (average over all other oceans) is also briefly
95 discussed in that section. A synthesis of the results is presented in the Discussion section
96 (section 0) with some highlights on the few main messages arising from this study.

97 **2 Data and methods**

98 **2.1 Data**

99 *2.1.1 Altimetry-based total sea level*

100 Sea level variations have been continuously measured by satellite altimetry since 1993. In this
101 study, we use the daily $0.25^\circ \times 0.25^\circ$ gridded sea level anomaly data, version DT2021 available
102 from the Copernicus Climate Change Service (C3S) (<https://cds.climate.copernicus.eu/>). The
103 data set is further corrected for the TOPEX-A instrumental drift that affected the first 6 years
104 of the time series, but the correction has no impact on our assessment that starts in 2004. The



105 Jason-3 radiometer drift that impacts the wet troposphere correction (Brown et al., 2023) is
106 corrected for. The altimetry data set is also corrected for the absolute Glacial Isostatic
107 adjustment (GIA) effect, using the ICE6G-D model from Peltier et al. (2018).

108 *2.1.2 GRACE-based ocean mass*

109 The Gravity Recovery and Climate Experiment (GRACE) and GRACE Follow-On (GRACE-
110 FO) are joint missions by the National Aeronautics and Space Administration (NASA) and the
111 German Aerospace Center (DLR) (Tapley et al., 2019). These satellites have been measuring
112 temporal variations in Earth's gravity field since 2002. This data set is essential for estimating
113 mass redistribution in the oceans, terrestrial water storage, ice sheets, and glaciers.
114 GRACE/GRACE-FO data are generally available in two forms: Spherical Harmonic (SH)
115 coefficients and Mass Concentration (mascon) solutions. In this study, we utilize the latest
116 Release 6 (RL06) mascon solutions provided by three different institutions: the Center for
117 Space Research (CSR), the Jet Propulsion Laboratory (JPL), and the German Research Centre
118 for Geosciences (GFZ). These mascon solutions, at monthly temporal resolution, are corrected
119 for the geocentric motion (degree-1) using the Sun et al. (2016) solution. The C_{20} and C_{30}
120 coefficients are derived from Satellite Laser Ranging (SLR) data. The GIA correction for
121 GRACE is based on the ICE6G-D model from (Peltier et al. (2018). Additionally, the GAD
122 product derived from AOD1B models (Dobslaw et al., 2017; Flechtner et al., 2014), which
123 represents non-tidal atmospheric and oceanic mass redistribution, is added back over the ocean
124 areas to restore the ocean bottom pressure, which combines the effects of ocean mass and
125 atmospheric loading. For alignment with altimetry-based sea level data which are corrected for
126 the inverse barometer, we remove the global mean atmospheric pressure at every grid mesh in
127 GRACE/GRACE-FO ocean mass data using the spatial mean of the GAD product at each
128 month (Chen et al., 2019). In this study, we both use individual mascon solutions as well as
129 their ensemble mean.



130 *2.1.3 Argo-based gridded data*

131 The Argo program is an international observational network that deploys a global array of
132 autonomous profiling floats to measure temperature and salinity in the upper 2000m of the
133 ocean. Several institutions process the raw data from these floats and publish gridded
134 temperature (T) and salinity (S) data. In this study, we utilize three distinct gridded products:
135 the Scripps Institution of Oceanography (SIO, Roemmich and Gilson, 2009), the Japan Agency
136 for Marine-Earth Science and Technology (JAMSTEC, Hosoda, 2007), and the Met Office
137 Hadley Centre (EN4 product, version 2.2, Cheng et al., 2014). Note that the SIO product rejects
138 salinity profiles exceeding a difference of 0.1 psu when comparing to historical estimate based
139 on the WOCE Global Hydrographic Climatology (Roemmich and Gilson, 2009). This
140 correction tends to withdraw the salinity drift reported in Argo floats since 2016 (Liu et al.,
141 2020; Ponte et al., 2021; Wong et al., 2023). Note that the other two products do not apply such
142 a correction. All three data products are available at <https://argo.ucsd.edu/data/data-access/>
143 (downloaded in October 2025). The thermosteric, halosteric and total steric sea level time series
144 are computed from these gridded temperature and salinity data using the Gibbs SeaWater
145 (GSW) Oceanographic Toolbox (McDougall et al., 2011) which implements the 2010
146 Thermodynamic Equation Of Seawater (TEOS-10) standard. The gridded Argo-based time
147 series have a spatial resolution of $1^{\circ} \times 1^{\circ}$ at monthly interval over January 2004 to December
148 2022.

149 *2.1.4 Ocean reanalyses*

150 We also used two ocean reanalysis data sets: (1) the CNR-ISMAR Global Historical Reanalysis
151 (CIGAR, Storto and Yang, 2024), and (2) the Ocean Reanalysis System 5 (ORAS5, Zuo et al.,
152 2019) available from the Copernicus Climate Change Service
153 (<https://www.copernicus.eu/en/copernicus-services>).



154 CIGAR is a reanalysis system developed by Storto and Yang (2024). It is based on the NEMO
155 ocean model version 4.0.7 (<https://www.nemo-ocean.eu/>) and is forced by the ECMWF ERA5
156 atmospheric reanalysis (<https://www.ecmwf.int/en/forecasts/dataset/ecmwf-reanalysis-v5>).
157 The system uses a three-dimensional variational (3D-Var) scheme to assimilate in situ profiles
158 from the EN4 data set. Notably, CIGAR does not assimilate satellite altimetry data, which
159 allows for independent comparisons. The system consists of 32 ensemble members generated
160 through varying configurations (e.g., perturbed initial conditions and atmospheric forcing). In
161 this study, we use the ensemble mean of the 32 members to derive the thermosteric, halosteric
162 and steric sea level.
163 The ORAS5 ocean reanalysis is based on the NEMO model (v3.4.1) and uses the NEMOVAR
164 data assimilation system. It assimilates a wide range of observations, including satellite
165 altimetry and sea surface temperature, at an eddy-permitting resolution of $0.25^{\circ} \times 0.25^{\circ}$.

166 **2.2 Methods**

167 *2.2.1 Computation of the manometric component*

168 In this study, we utilize two methods to obtain an estimate of the manometric component. One
169 method is to use the ensemble mean of the GRACE mascon solutions from CSR, JPL, and
170 GSFC to obtain the GRACE-based manometric estimate. The other method, an alternative to
171 using GRACE solutions, relies on ocean reanalysis data and follows the approach developed
172 by Camargo et al. (2023). Here, we use the sterodynamic sea level provided by the CIGAR
173 ocean reanalysis, which combines the global mean thermosteric and dynamic sea level changes.
174 To isolate the manometric component, we subtract the local steric effect from the sterodynamic
175 sea level and further add the contemporary Gravitational, Rotational, and Deformation (GRD)
176 fingerprints (representing solid Earth deformations and gravitational effects due to present-day
177 land ice melt and terrestrial water storage changes; Gregory et al., 2019), to obtain a
178 manometric component comparable to GRACE. The sea level fingerprint data used in this



179 study are based on monthly GRD fingerprint grids (0.5×0.5 resolution) estimated by Adhikari
180 et al. (2019). Since this original dataset ends in 2016, we extended the time series up to 2022
181 using linear extrapolation, assuming that the observed trend remains constant after 2016 (see
182 Bouih et al., 2025 for details). This reanalysis-based estimate is hereafter referred to as CIGAR
183 manometric. Manometric sea level change generally refers to the sea level component
184 associated with ocean mass variations (i.e., excluding the steric component). It is driven by
185 water mass exchange with the continents (such as land ice melt and terrestrial water storage
186 changes) as well as mass redistribution within the ocean, driven by ocean circulation. However,
187 in the context of this study, we focus exclusively on the internal mass redistribution component
188 (with the global mean ocean mass trend removed). Therefore, the 'manometric sea level' here
189 refers solely to the redistribution by the ocean circulation, of water mass already present in the
190 oceans, with the GRDs effect added as explained above.

191

192 *2.2.2 Post processing of the data*

193 To ensure spatial consistency across all observing systems, all gridded data sets were spatially
194 interpolated onto a $1^\circ \times 1^\circ$ grid and averaged at monthly interval. A three-month moving
195 average filter was applied to the time series. For the spatial analysis, a common mask was
196 applied to all gridded components to exclude regions with high uncertainty. This mask covers
197 latitudes from 66°S to 66°N , excludes inland seas, and omits coastal regions where the distance
198 from land is less than 300 km (see Bouih et al., 2025 for details). Seasonal signals (annual and
199 semi-annual) are removed from the time series through a least-squares adjustment of 6 and 12-
200 month sinusoids. For the spatial maps, this least-squares fit was used to calculate the trends at
201 each grid point. Finally, the globally averaged trend of each data set computed over the study
202 period was subtracted from each grid point before constructing the spatial trend maps to focus
203 on regional spatial patterns. The study period spans from January 2004 to December 2022.



204 2.2.3 Data uncertainties

205 For the altimetry grids, we use the uncertainties estimated by Prandi et al. (2021). For the
206 GRACE-based manometric component, uncertainties are derived from the dispersion of the
207 data sets with respect to the ensemble mean. For the CIGAR-based manometric, thermosteric,
208 halosteric and steric data, the dispersion of the 32 realizations around the ensemble mean was
209 used to estimate the uncertainties. For the residual time series, the uncertainty was estimated
210 using the law of error propagation, considering all terms of the sea level budget. Regarding the
211 trend uncertainty, it is expressed as the standard error of the least-squares fit. To obtain the
212 uncertainty at the 95% confidence level, we scaled the standard error by a factor of 2
213 (representing the 2-sigma interval).

214 3 Results

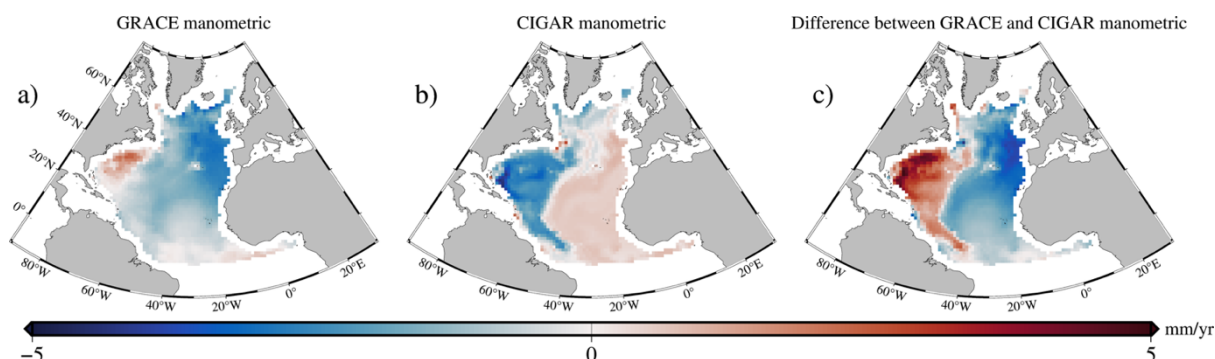
215 3.1 Comparison of the different manometric components over the North Atlantic

216 Figure 1a, b, shows the spatial manometric trend in the North Atlantic using the GRACE and
217 CIGAR manometric data. Comparing Figure 1(a) and (b), we observe distinctly contrasting
218 patterns between the GRACE and CIGAR manometric components. For the GRACE-based
219 component, significant negative trends dominate most of the basin, with magnitudes gradually
220 weakening from east to west. However, positive trends are observed in the western tropical
221 Atlantic. In contrast, the CIGAR manometric component displays positive trends in the east
222 and negative trends in the west, separated by a distinct dividing line, which likely corresponds
223 to the position of the Mid Atlantic Ridge. This contrast is clearly illustrated Figure 1c, which
224 plots the difference between the GRACE and CIGAR estimates. The results indicate that the
225 GRACE manometric trends are larger than those of CIGAR west of 40°W, particularly along
226 the eastern coast of North America. Conversely, in the region east of 40°W, the GRACE



227 manometric trends are smaller than the CIGAR trends, with the most significant difference
228 observed near Greenland.

229



230

231 *Figure 1. Manometric sea level trends in the North Atlantic over 2004.01-2022.12 derived from*
232 *(a) the mean of three GRACE mascon solutions and (b) the CIGAR ocean reanalysis. (c)*
233 *Difference between (a) and (b).*

234

235 **3.2 Comparison of the different steric products over the North Atlantic**

236 Figure 3a-c shows the thermosteric sea level (TSL) trends over 2004-2022 over the North
237 Atlantic for the three Argo products SIO, JAMSTEC and EN4. Similarly, Figure 3d-f shows
238 the halosteric sea level (HSL) trends for the same data sets and period. As expected, due to
239 thermohaline compensation particularly strong in the North Atlantic (e.g., Pardaens et al., 2011;
240 Wang et al., 2010; Wunsch et al., 2007), the two components display opposite trends.
241 Regarding the thermosteric component (Figure 3a-c), while all three products display similar
242 spatial patterns, their magnitudes vary. The JAMSTEC and EN4 products show stronger
243 positive trends around 20°N compared to the SIO product. However, all three products indicate
244 significant positive signals in the eastern North Atlantic. The three halosteric products share
245 similar spatial patterns; however, the magnitude of the SIO product is notably smaller than for
246 JAMSTEC and EN4, the latter two being very similar. This difference likely results from the

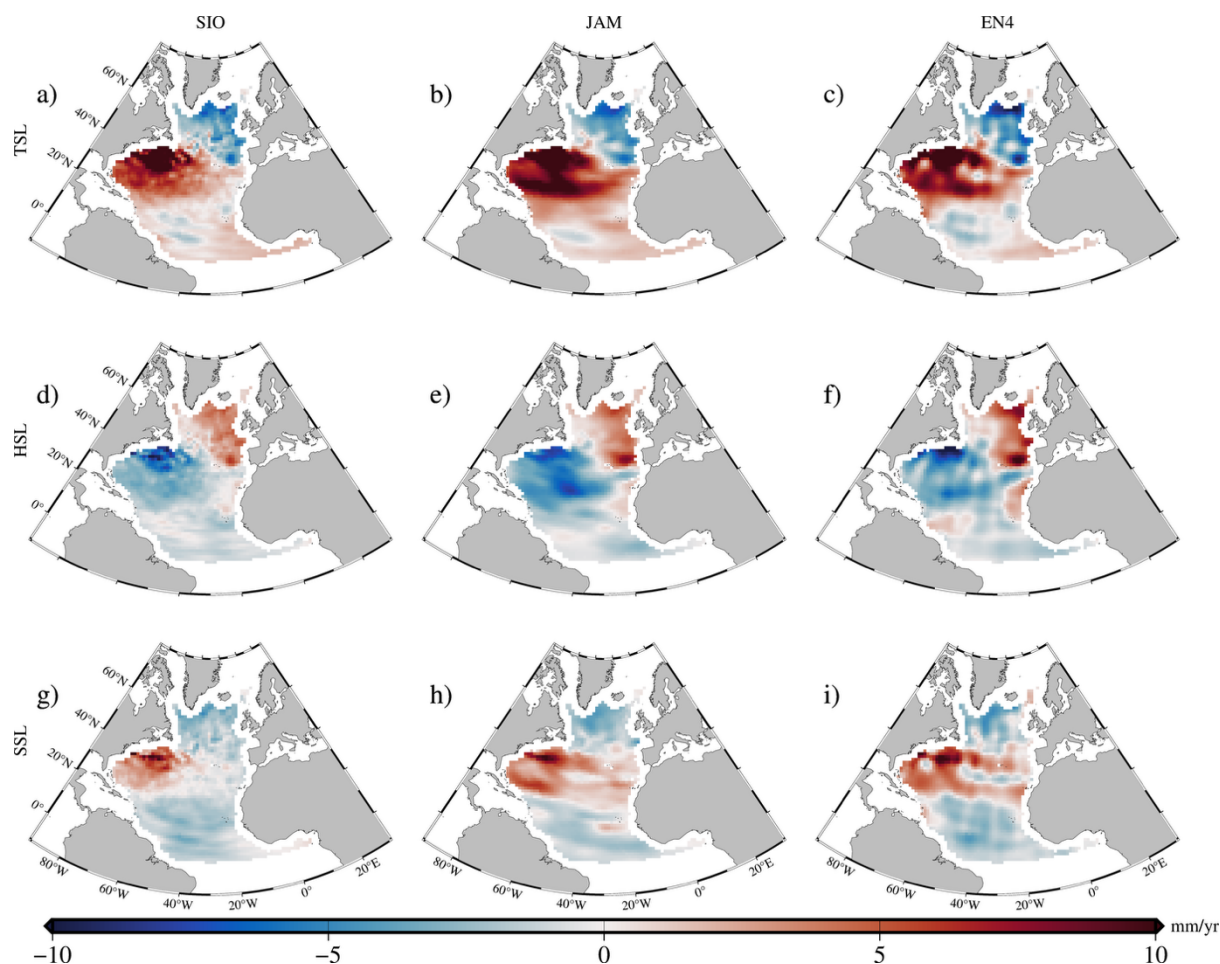


247 SIO processing that corrects for the instrumental salinity drift reported in Argo floats since
248 2016, whereas the other products may not account for this. The mapping methods used by the
249 different processing groups, in particular the assumed different correlation radii, may also
250 contribute to the observed differences.

251 The steric sea level (SSL) trends are shown in Figure 3g-i. The magnitude of the total steric
252 change is smaller than that of the thermosteric component alone. This implies that the halosteric
253 contribution plays a significant compensatory role in the North Atlantic (consistent with
254 previous published studies (e.g., Bouih et al., 2025; Llovel and Hochet, 2025). Unlike in the
255 case of the global mean, the influence of salinity changes on sea level cannot be ignored in this
256 region.

257

258



260 *Figure 2. Trends of thermosteric (a–c), halosteric (d–f), and steric (g–i) sea level change in*
261 *the North Atlantic over 2004–2022 derived from the SIO (a, d, g), JAMSTEC (b, e, h), and EN4*
262 *(c, f, i) Argo products.*

263

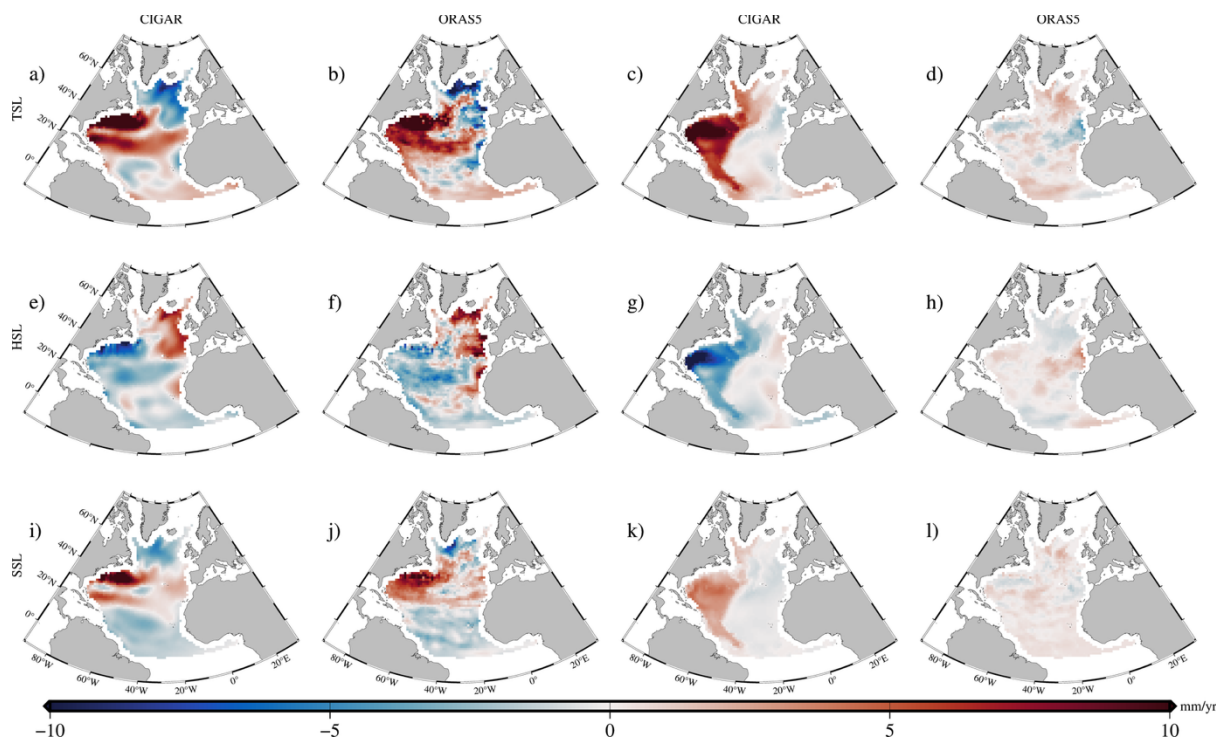
264 3.2.1 Ocean reanalyses-based thermosteric, halosteric and steric products

265 In addition to Argo products, we used the CIGAR and ORAS5 ocean reanalysis data to compute
266 thermosteric, halosteric, and steric sea level changes for both the upper 2000m and the deep



267 ocean (2000m-6000m), as shown in Figure 3. In the upper 2000m, CIGAR and ORAS5 exhibit
268 similar spatial patterns across all three components. Notably, the thermosteric sea level change
269 displays a significant signal in the western North Atlantic, consistent with the Argo-based
270 results. However, marked discrepancies between the two reanalyses are evident below 2000m.
271 The CIGAR product displays strong positive thermosteric and negative halosteric signals in
272 the western North Atlantic compared to ORAS5. In contrast, the deep ocean signals in ORAS5
273 are weak and spatially incoherent, with some areas showing even signs opposite to those
274 observed in the upper 2000m. Consequently, the spatial patterns in CIGAR, triggered by
275 vertical physics and, to a lesser extent, vertical error correlations embedded in the 3D-Var
276 scheme, appear more consistent with the upper 2000m than those in ORAS5.

277



278

279 *Figure 3. Trends of thermosteric (a–d), halosteric (e–h), and steric (i–l) sea level change in*
280 *the North Atlantic over 2004–2022. The panels compare contributions from the upper 2000 m*



281 *(a, b, e, f, i, j) and below 2000 m (c, d, g, h, k, l) derived from the CIGAR (a, c, e, g, i, k) and*
282 *ORAS5 (b, d, f, h, j, l) reanalyses.*
283

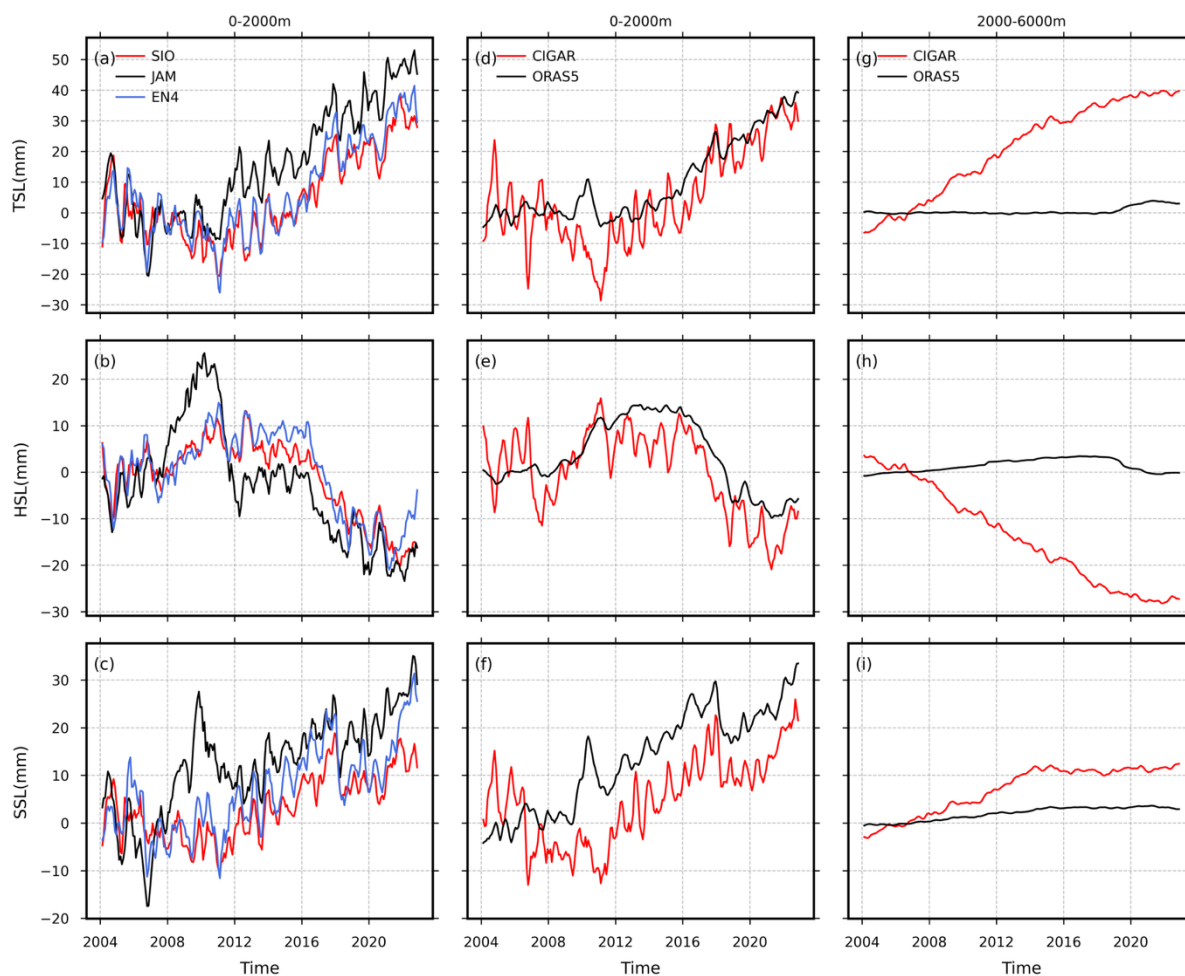
284 *3.2.2 Argo-based and ocean reanalysis thermosteric, halosteric and steric time series*

285 Next, we examine the thermosteric, halosteric and steric time series (weighted averages of the
286 gridded data in the North Atlantic) for the different Argo and ocean reanalysis product (Figure
287 4). Figure 4a,d indicate that the thermosteric component exhibits an upward trend in all
288 products, although the rates of rise vary. Regarding the halosteric component (Figure 4b,e), we
289 observe that the SIO and CIGAR products show a small decreasing trend that begins earlier
290 than 2016, which may represent a true physical salinity increase during this early period.
291 Among the three Argo products (Figure 4a-c), SIO and EN4 show strong agreement in
292 thermosteric, halosteric, and steric sea level changes. In contrast, JAMSTEC deviates from the
293 other two products, particularly in the halosteric component, which displays an unrealistic
294 increase during the 2010s. Consequently, this discrepancy causes the total steric sea level
295 change in JAMSTEC to mismatch with the other two products. In the following, we exclude
296 the JAMSTEC product from the subsequent analysis.

297 Figure 4d-i presents the changes for CIGAR and ORAS5 in the upper 2000m ocean depth and
298 from 2000m to 6000m (deep ocean). In the upper 2000m, Although there is a little difference
299 in trend before 2010, they are consistent across components after 2010, although their
300 amplitudes slightly differ. However, in the deep ocean (2000–6000m), substantial
301 discrepancies exist between the two products. As mentioned above, ORAS5 exhibits a weak
302 signal in the deep ocean; its thermosteric trend is nearly zero until 2019. In contrast, CIGAR
303 shows a consistent and distinct upward trend. Regarding the halosteric change, ORAS5 shows
304 a weakly rising trend until 2019, whereas CIGAR shows a consistent and obvious decrease.
305 Finally, while both products exhibit rising trends in steric sea level change in the deep ocean,
306 their magnitudes differ significantly. Given the unrealistically stationary thermosteric signal

307 observed in ORAS5 below 2000m, we suspect that this product is unreliable in its deep ocean
308 variability.

309



310

311 *Figure 4. Time series of thermosteric (a, d, g), halosteric (b, e, h), and steric (c, f, i) sea level*
312 *change in the North Atlantic. Panels (a–c) show the upper 2000 m derived from Argo products*
313 *(SIO, JAM, EN4), while panels (d–i) are derived from CIGAR and ORAS5 reanalyses for the*
314 *upper 2000 m (d–f) and the deep ocean 2000–6000 m (g–i). All time series have applied three-*
315 *month moving average filtering. Global mean trend is included.*

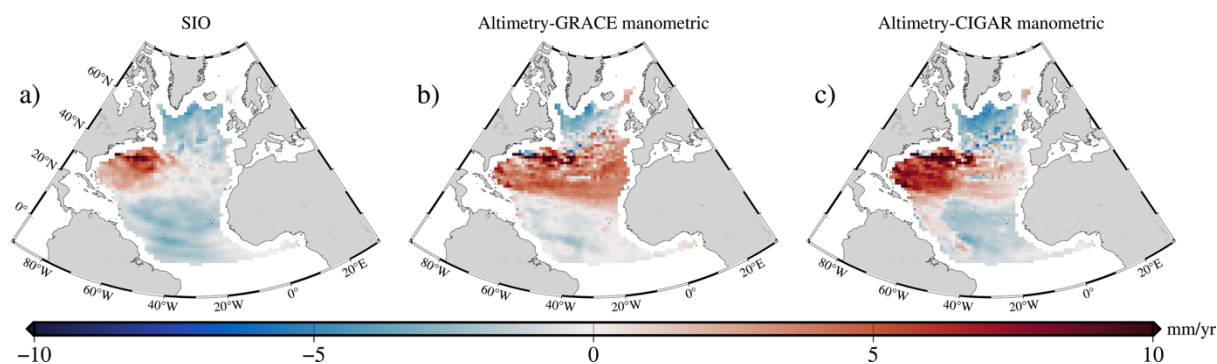


316 **3.3 Comparison between the SIO steric trends and altimetry sea level trends corrected for**
317 **the manometric component**

318 In addition to directly obtaining the steric sea level trends, we can also derive it indirectly using
319 the sea level budget equation (i.e., altimetry sea level minus manometric component computed
320 at each grid mesh of the gridded products). In Figure 5, we compare the direct steric estimate
321 from SIO with indirect estimates derived by subtracting different manometric products
322 (GRACE or CIGAR) from altimetry trend data. It is important to note that the indirect method
323 inherently includes deep ocean contribution and relies on independent observations.

324 From Figure 5, we clearly observe that the spatial trend pattern of SIO is more consistent with
325 the “Altimetry minus CIGAR manometric” estimate, as both exhibit positive signals in the
326 western North Atlantic. In contrast, the “Altimetry minus GRACE manometric” estimate
327 displays a prominent positive signal in the eastern North Atlantic which is absent in the SIO
328 data. This suggests that the GRACE manometric data contains substantial inaccuracies,
329 particularly in the eastern North Atlantic, while “Altimetry minus CIGAR manometric” agrees
330 rather well with the SIO steric trends.

331



332

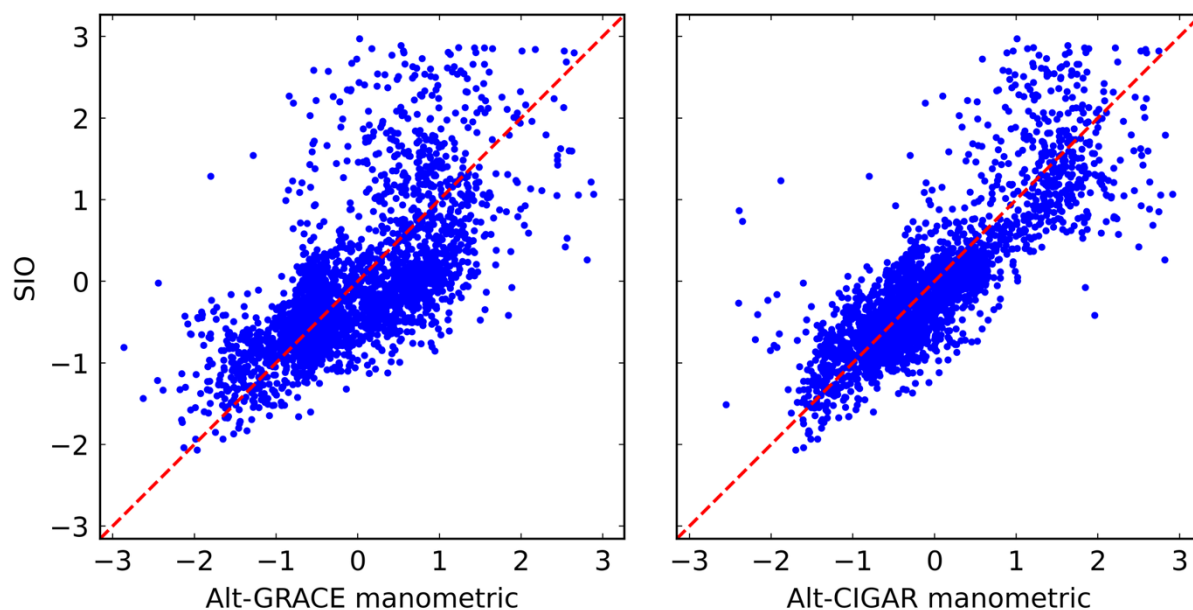
333 *Figure 5. Steric sea level trends derived directly from SIO and indirectly from Altimetry minus*
334 *manometric estimates (GRACE or CIGAR).*

335



336 To highlight this further, Figure 6a, b shows the scatter plots between SIO gridpoint steric
337 trends and “Altimetry minus GRACE manometric” and “Altimetry minus CIGAR manometric”
338 grid point trends.

339 The scatter plots reveal distinct differences in the correlation between SIO observations and
340 the two manometric estimates. In the negative SIO region (corresponding to the lower half of
341 Figure 6 and the negative values regions in Figure 5), where most points align with the diagonal
342 in both cases, the ‘Altimetry-CIGAR manometric’ points are clustered notably more tightly
343 than those in the ‘Altimetry-GRACE manometric’ comparison. This indicates that in regions
344 with negative steric sea level change, where both estimates correlate with SIO, the “Altimetry-
345 CIGAR manometric” estimate maintains a higher spatial correlation compared to “Altimetry-
346 GRACE manometric”. In the positive SIO areas (corresponding to the upper half of the plots),
347 a portion of the data points in both estimates exhibit values lower than the SIO observations
348 (indicated by points falling above the diagonal). However, this underestimation is much more
349 pronounced for ‘Altimetry-GRACE manometric’, leading to a larger spread away from the
350 diagonal compared to Altimetry-CIGAR manometric. This suggests that while the correlation
351 with SIO decreases for both products in positive steric sea level trend regions (such as the
352 western North Atlantic), the correlation of “Altimetry-GRACE” is notably weaker than that of
353 “Altimetry-CIGAR manometric”.



354

355 *Figure 6. Scatter plots of SIO steric sea level change versus Altimetry minus manometric*
356 *estimates (GRACE/left or CIGAR/right). The data have been normalized and outliers*
357 *exceeding 3σ were removed.*

358

359 **3.4 Residual trend maps in the North Atlantic**

360 In this section, we utilize data from the observing systems described above to compute spatial
361 maps of the sea level budget residuals.

362 *3.4.1 North Atlantic budget residuals of different manometric and steric (0-2000m)* 363 *components*

364 We computed the residuals by subtracting various combinations of manometric (GRACE,
365 CIGAR) and steric (SIO, EN4, CIGAR, and ORAS5 upper 2000 m) components from the
366 altimetry data (Figure 7).

367 As shown in Figure 7a,e, the resulting residuals implicitly include a deep ocean steric
368 contribution, which is not accounted for since the steric data are limited here to the upper 2000



369 m. This is consistent with previous results from Bouih et al. (2025), who observed positive
370 residuals in the North Atlantic for both manometric cases., Similarly positive residuals are
371 found in the eastern North Atlantic for the GRACE manometric component and in the western
372 North Atlantic for the CIGAR manometric component.

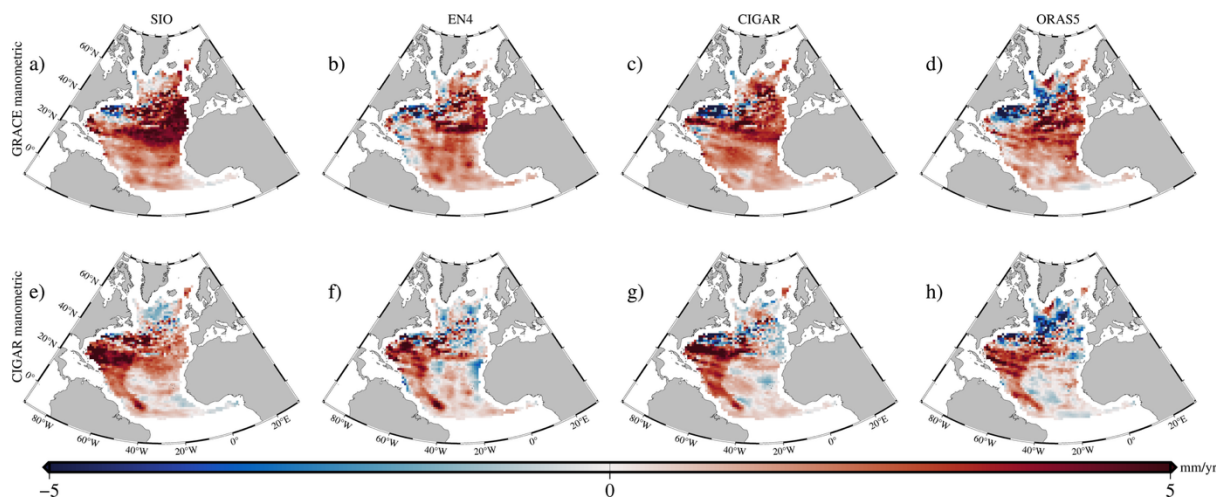
373 From Figure 7, we also observe that the spatial distribution of the residuals remains similar
374 when the manometric component is held fixed while varying the steric components. However,
375 the residual magnitude is different. Specifically, when using the GRACE manometric
376 component, the positive signal derived from SIO is stronger in the eastern North Atlantic
377 compared to other steric products. When using the CIGAR manometric component, the
378 positive signals from SIO and CIGAR are stronger in the western North Atlantic compared to
379 EN4 and ORAS5.

380 To quantify the residuals, we computed the latitude-weighted spatial mean trend of each map.
381 Results are shown in Table 1 (remind that results in Table 1 do not account for the global mean
382 trends). From Table 1, we observe that regardless of the steric data used (whether from Argo
383 or ocean reanalyses), the residuals derived using the CIGAR manometric component are
384 always smaller than those derived using GRACE. Furthermore, for a given manometric
385 component, the residual with SIO is larger than that with EN4, even though SIO has corrected



386 for the salinity drift since 2016. Besides, the residual with CIGAR steric is larger than that with
 387 ORAS5.

388



389

390 *Figure 7. Maps of sea level residuals in the North Atlantic. The residuals are calculated by*
 391 *subtracting manometric and steric components from satellite altimetry. The manometric*
 392 *component is derived from GRACE (a–d) and CIGAR (e–h). These are combined with upper*
 393 *2000 m steric estimates from SIO (a, e), EN4 (b, f), CIGAR (c, g), and ORAS5 (d, h).*

394

395

396 *Table 1. Trend values (mm/yr) of sea level residuals in the North Atlantic corresponding to*
 397 *different steric products (0–2000m) and the two manometric components. Global mean trends*
 398 *were removed. Uncertainties are 2-sigma errors of the least-squares fit.*

399

Trend (mm/yr)	SIO	EN4	CIGAR	ORAS5
GRACE manometric	2.15±0.19	1.43±0.22	1.52±0.21	1.10±0.20
CIGAR manometric	1.50±0.23	0.77±0.23	0.86±0.25	0.45±0.16

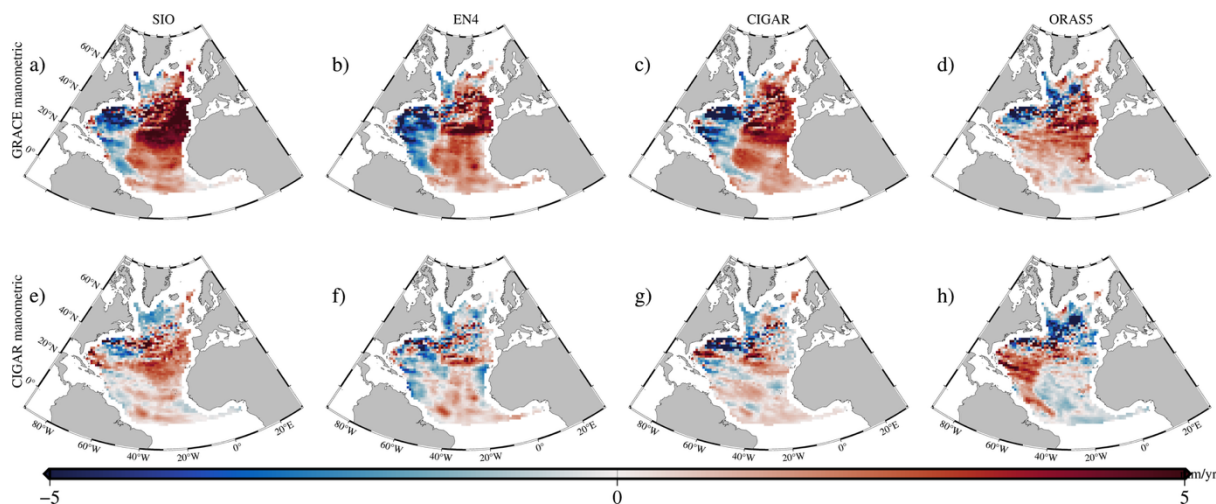
400



401 *3.4.2 North Atlantic budget residuals and deep ocean steric contribution*

402 In this section, we added the deep ocean steric sea level change to the upper 2000 m steric
403 estimates, considering both the CIGAR and ORAS5 deep steric data, and using either GRACE
404 or CIGAR for the manometric components. Resulting residual trends are shown in Figure 8 .
405 For all cases except the ORAS5 deep ocean case, the residuals derived using GRACE
406 manometric data (Figure 8a–c) show a dipole pattern (positive in the east, negative in the west)
407 compared to the results without the deep ocean component (Figure 7). Table 2 summarizes the
408 residual trend values for all cases (as for Table 1, remind that results in Table 2 do not account
409 for the global mean trends). Comparing results from Table 1 and Table 2, we note that the mean
410 residual magnitude is significantly reduced when the deep ocean steric change is included: by
411 ~30% when using GRACE for the manometric component and SIO for the upper 0–2000m
412 steric sea level, and by ~50% when using CIGAR for both the steric (full depth and manometric
413 component). Based on CIGAR, the deep steric contribution to the North Atlantic sea level
414 budget (in addition to the global mean deep ocean contribution) amounts to 0.62 ± 0.04 mm/yr.
415 In contrast, when using the CIGAR manometric component (Figure 8e–h), the residuals
416 decrease significantly in both spatial variability and magnitude. Notably, the sea level budget
417 is effectively nearly closed within error bars when combining CIGAR manometric and CIGAR
418 steric data. Finally, it is worth noting that for SIO, positive residuals are observed in the eastern
419 North Atlantic regardless of whether GRACE or CIGAR manometric data is used.

420



421

422 *Figure 8. Maps of sea level residuals in the North Atlantic, calculated as in Figure 7 but with*
 423 *the inclusion of the deep ocean (below 2000 m) steric component. The deep ocean contribution*
 424 *is derived from CIGAR for panels (a–c, e–g) and from ORAS5 for panels (d, h). In panels a–c,*
 425 *the manometric component is from GRACE while it is from CIGAR in panels e–h.*

426

427 *Table 2. Trend values (mm/yr) of sea level residuals in the North Atlantic for four steric*
 428 *products and two manometric components. For SIO and EN4, the deep ocean contribution*
 429 *from CIGAR is added. For CIGAR and ORAS5, their own deep steric contributions are*
 430 *considered. Global mean trends removed. Uncertainties are 2-sigma errors of the least-*
 431 *squares fit.*

432

Trend (mm/yr)	SIO	EN4	CIGAR	ORAS5
GRACE manometric	1.53 ± 0.21	0.81 ± 0.24	0.90 ± 0.23	0.87 ± 0.20
CIGAR manometric	0.88 ± 0.20	0.15 ± 0.21	0.24 ± 0.22	0.22 ± 0.15

433 3.5 Time series of the North Atlantic mean sea level budget

434 Based on the analysis above, the deep ocean contribution to the North Atlantic sea level budget
 435 cannot be ignored. To assess the influence of the deep ocean on the sea level budget, we



436 computed time series for each component, including total sea level, manometric sea level,
437 thermosteric sea level, and halosteric sea level. Compared to results discussed above, here we
438 account for the global mean trend of each component.

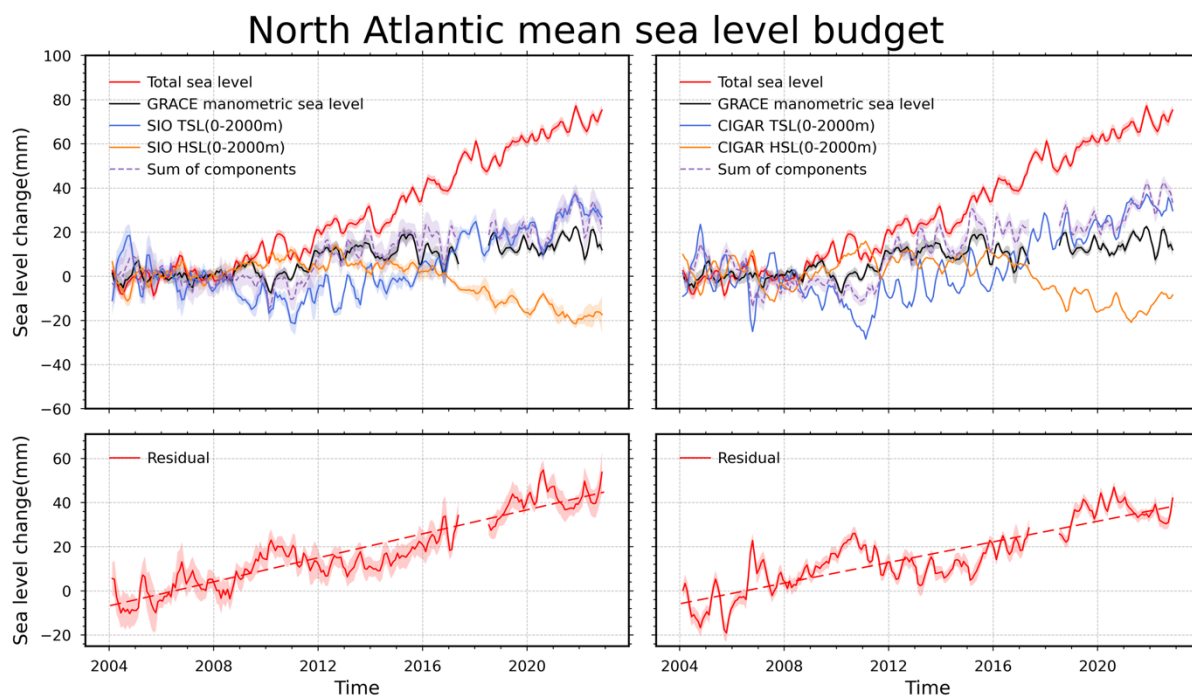
439 *3.5.1 North Atlantic mean sea level budget time series without deep ocean (global mean trends*
440 *included)*

441 Here, we have reintroduced the global mean trend of each component. Since the CIGAR
442 manometric component does not fully account for the external sea water mass addition to the
443 ocean due to land ice melt and terrestrial waters, we adopt GRACE data to represent the total
444 manometric sea level change (i.e., global mean trend accounted for). Regarding the steric sea
445 level component, we selected the SIO product for Argo estimates, as it corrects for the salinity
446 drift. For ocean reanalyses, we only consider the CIGAR reanalysis.

447 Figure 9 presents the sea level budget time series (global mean trends accounted for) in the
448 North Atlantic without the deep ocean steric sea level change. Residual time series are also
449 shown. The left/right panels use SIO/CIGAR steric sea level change in upper 2000m.
450 Comparing Figure 9 left and right panels, we observe that the halosteric components from SIO
451 and CIGAR slightly differ. For SIO, a slight halosteric decrease is observed over 2012-2015,
452 with a linear trend of -1.10 ± 0.94 mm/yr during the such period, then it increases to -3.20 ± 0.9
453 mm/yr over 2016-2022. Consequently, the SIO halosteric trend over 2012-2022 amounts to -
454 2.87 ± 0.21 mm/yr. In terms of global mean trend, the SIO halosteric time series does not show
455 any trend (as expected since the salinity drift is supposed to be corrected). Thus, the SIO
456 halosteric decrease observed in the North Atlantic may possibly reflect a truly physical salinity
457 increase. As of 2016, the CIGAR halosteric decrease is slightly larger than for SIO, possibly a
458 consequence of the salinity drift error not corrected for in the assimilated EN4 salinity data.
459 The mean residual trends amount to 2.72 ± 0.19 mm/yr and 2.34 ± 0.21 mm/yr for the SIO and
460 CIGAR steric cases respectively, i.e., not significantly different.



461



462

463 *Figure 9. Time series of North Atlantic sea level components (top) and residuals (bottom) for*
464 *the upper 2000m. The analysis uses Altimetry and GRACE manometric data, combined with*
465 *steric estimates from SIO (left) and CIGAR (right). All time series have applied three-month*
466 *moving average filtering. The global mean trend of each component is included.*

467

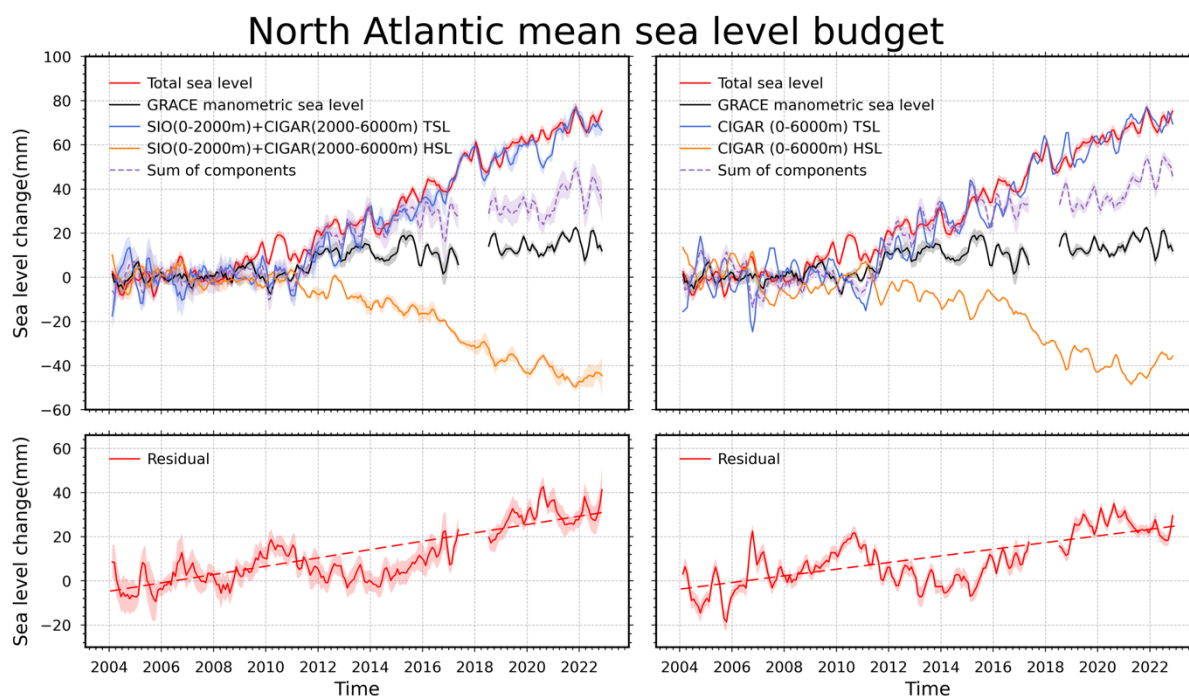
468 *3.5.2 North Atlantic sea level budget time series with the deep ocean contribution (global mean*
469 *trends included)*

470 In this section, we add the deep ocean contribution from the CIGAR reanalysis. As in section
471 3.5.1, the GRACE manometric component is considered, and for the upper 2000m steric
472 component, both SIO and CIGAR data are used. The corresponding sea level budget time series
473 for the North Atlantic are shown in Figure 10.

474 As illustrated in Figure 10, with the inclusion of the deep ocean contribution, the halosteric
475 decline in both panels become more evident compared to the case without the deep ocean.



476 Specifically, the CIGAR component also shows a slight decrease starting in 2012. However,
477 unlike the SIO trend, which maintains a relatively stable decline throughout the study time span,
478 the CIGAR decrease still exhibits a sudden intensification after 2016. Similarly, the
479 thermosteric sea level also displays a stronger increasing trend compared to the case without
480 the deep ocean.
481 Consequently, the total steric sea level trend is larger than in the case without the deep ocean
482 contribution. Finally, the inclusion of the deep ocean contribution leads to a reduction in the
483 North Atlantic residual trends for both cases: for the estimate based on SIO (upper 2000 m),
484 the trend decreases by about 30%, from 2.72 ± 0.19 mm/yr to 1.89 ± 0.21 mm/yr, whereas for
485 the estimate based on CIGAR, it drops from 2.34 ± 0.21 mm/yr to 1.51 ± 0.23 mm/yr.
486



487
488 *Figure 10. Time series of North Atlantic sea level change components (top) and budget*
489 *residuals (bottom). The left panels use a hybrid steric estimate (SIO for 0–2000m combined*



490 *with CIGAR for 2000–6000m), while the right panels use the full-depth CIGAR steric estimate*
491 *(0–6000m). In both cases, Altimetry and GRACE manometric data are used. All time series*
492 *have applied three-month moving average filtering. The global mean trend of each component*
493 *is included.*

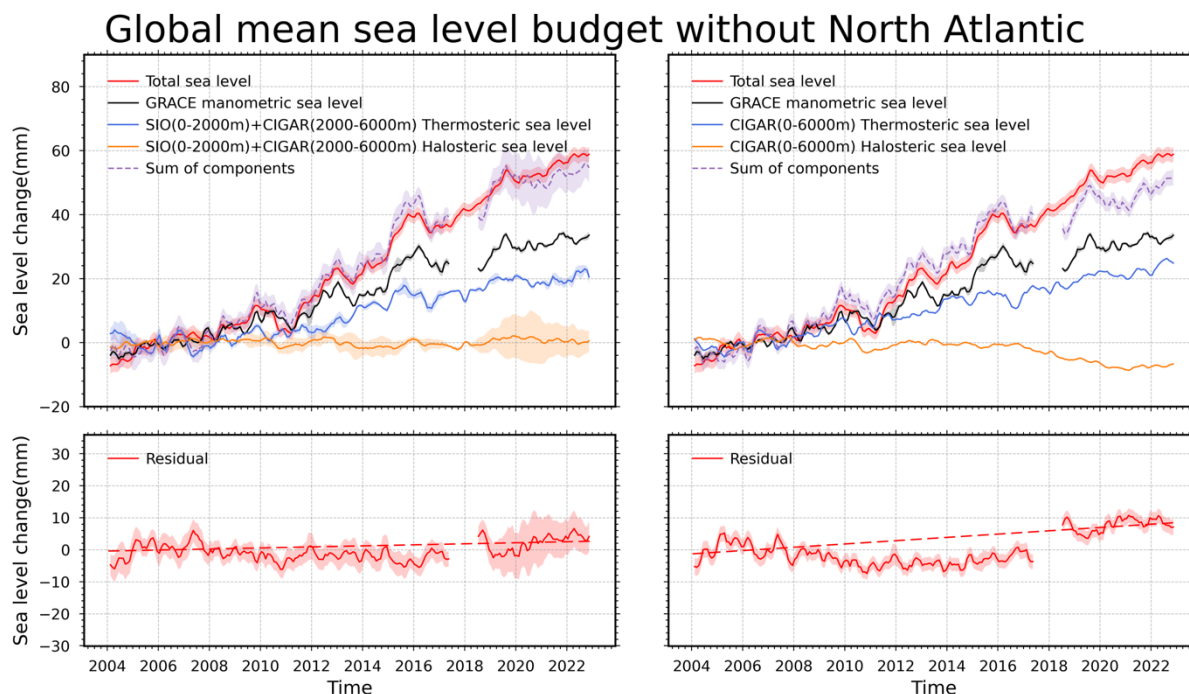
494

495 *3.5.3 Sea level budget of all oceans but without the North Atlantic Ocean, with the deep ocean*
496 *contribution added*

497 In Bouih et al. (2025)’s study, the sea level budget for the global ocean excluding the North
498 Atlantic (without the deep ocean steric contribution) was not closed. In this section, we
499 consider the deep ocean steric sea level change contribution to the sea level budget. We
500 compute the sea level budget for the global ocean excluding the North Atlantic using the same
501 data products as in Section 3.5.2. The corresponding results are shown in Figure 11.

502 In the left panel (using SIO data for the upper 2000 m), we observe that the halosteric sea level
503 change is nearly zero. The residual is very small, estimated at 0.16 ± 0.08 mm/yr. Thus,
504 considering the whole oceanic domain without the North Atlantic, the sea level budget is closed
505 when SIO data are used for the upper 2000 m ocean layer. In contrast, the right panel (using
506 CIGAR data for all depths) shows a distinct decrease in halosteric sea level starting in 2016,
507 due to the assimilation of EN4 data in CIGAR (not corrected for the salinity drift).
508 Nevertheless, the residual trend of the right panel is small (0.51 ± 0.11 mm/yr), suggesting quasi
509 closure of the sea level budget.

510



511

512 *Figure 11. Time series of sea level components (top) and residuals (bottom) for the global*
513 *ocean excluding the North Atlantic. The left panels use a hybrid steric estimate (SIO for 0–*
514 *2000 m combined with CIGAR for 2000–6000m), while the right panels use the full-depth*
515 *CIGAR estimate (0–6000m). All time series have applied three-month moving average filtering.*
516 *The global mean trend of each component is included.*

517

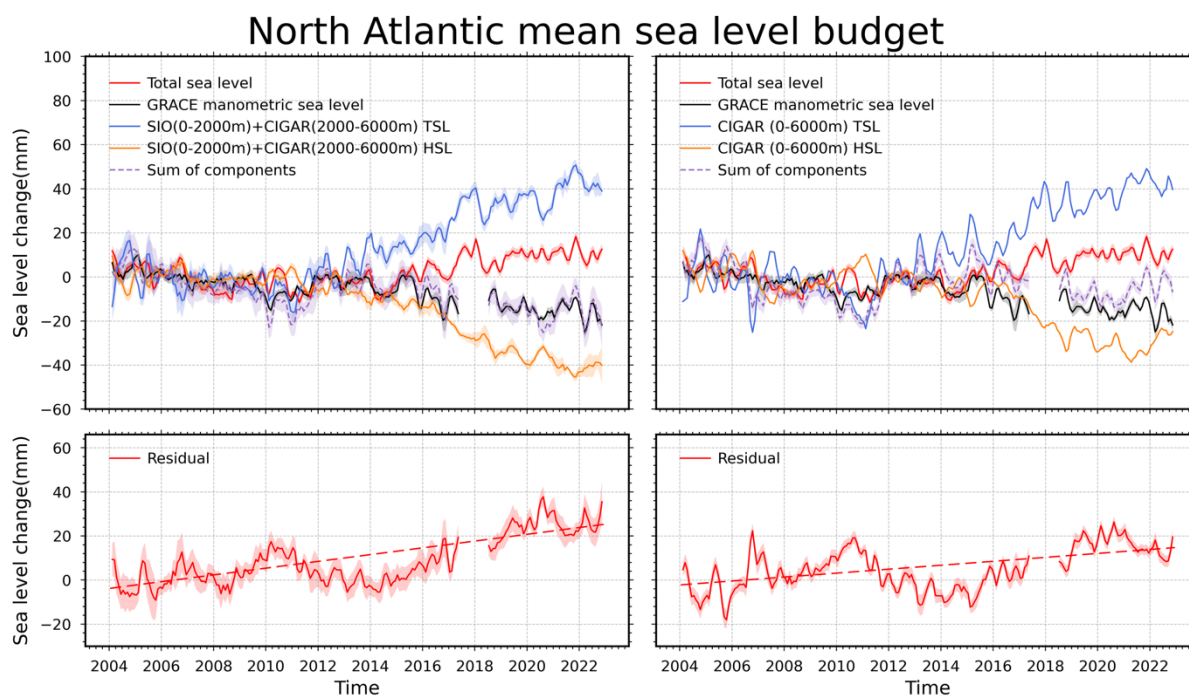
518 *3.5.4 North Atlantic sea level budget time series with the deep ocean contribution (global mean*
519 *trends removed)*

520 Here, we compute the North Atlantic sea level budget (including the deep ocean contribution)
521 with the global mean sea level trends of all components removed. The objective is to determine
522 which part of the non-closure in the North Atlantic budget may result from errors in the regional
523 components (i.e., independently from errors in the global mean trends). Figure 12 presents the
524 budget time series using GRACE for the manometric component. We consider two steric cases:
525 the hybrid case (SIO 0–2000 m plus CIGAR deep ocean) and the CIGAR full-depth case.



526 The mean residual trends are estimated at 1.53 ± 0.21 mm/yr for the hybrid steric case and
527 0.88 ± 0.20 mm/yr for the CIGAR full-depth case. Comparing these results (where global mean
528 trends are removed) with those in Figure 10 (where global mean trends are included), we
529 observe very little difference in the mean residual trends. This suggests that errors in the global
530 mean trends are small, and that the reported residuals in the North Atlantic budget are primarily
531 driven by component errors at the regional scale.

532

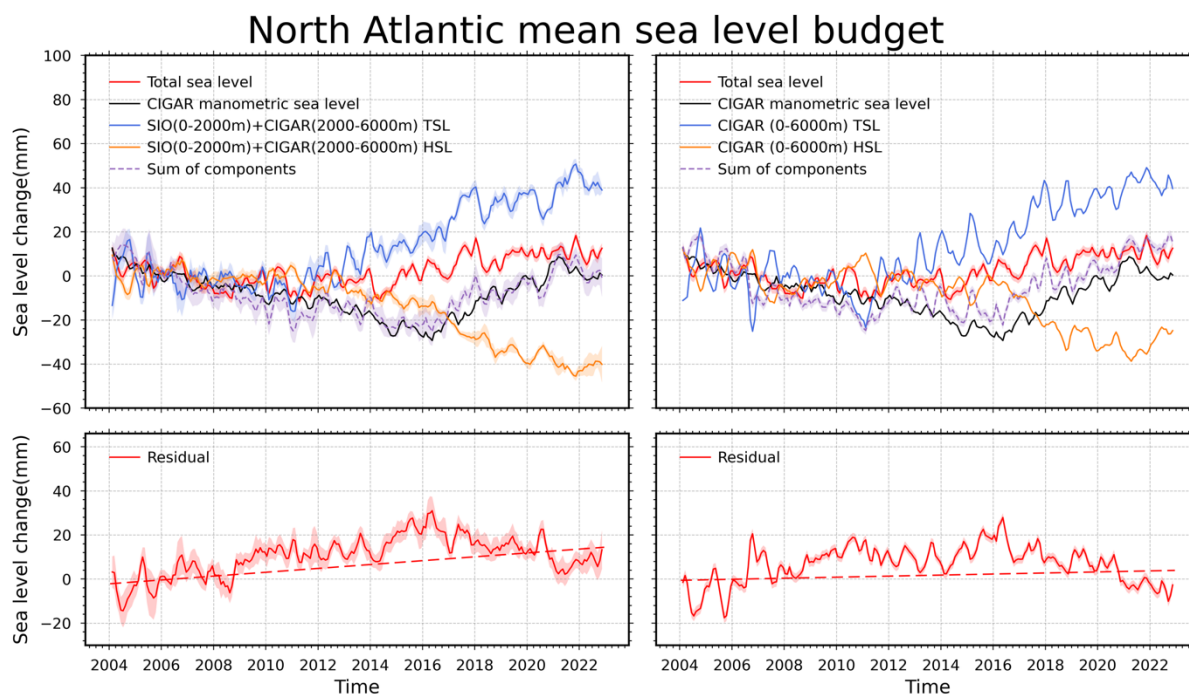


533

534 *Figure 12. Time series of North Atlantic sea level change components (top) and budget*
535 *residuals (bottom). The left panels use a hybrid steric estimate (SIO for 0–2000m combined*
536 *with CIGAR for 2000–6000m), while the right panels use the full-depth CIGAR steric estimate*
537 *(0–6000m). In both left and right panels, GRACE manometric components are considered. All*
538 *time series have applied three-month moving average filtering. The global mean trend of each*
539 *component is removed.*

540

541 Figure 13 displays the corresponding budget time series using CIGAR for the manometric
542 component. Similarly, we evaluate the residuals for both steric configurations. When using the
543 CIGAR manometric data, the mean residual trends amount to 0.88 ± 0.20 mm/yr for the hybrid
544 steric case (SIO 0–2000 m plus CIGAR deep ocean) and 0.24 ± 0.22 mm/yr for the CIGAR full-
545 depth case.
546



547

548 *Figure 13. Time series of North Atlantic sea level change components (top) and budget*
549 *residuals (bottom). The left panels use a hybrid steric estimate (SIO for 0–2000m combined*
550 *with CIGAR for 2000–6000m), while the right panels use the full-depth CIGAR steric estimate*
551 *(0–6000m). In both left and right panels, CIGAR manometric components are considered. All*
552 *time series have applied three-month moving average filtering. The global mean trend of each*
553 *component is removed.*
554

555 Comparing the results from Figure 12 and Figure 13, we note that using CIGAR for the
556 manometric component consistently leads to smaller regional residuals than using GRACE,



557 regardless of the steric product considered. It is worth noting that the configuration using
558 CIGAR for both manometric and steric components yields a mean residual trend of 0.24 ± 0.22
559 mm/yr, nearly four times smaller than in the case where the GRACE manometric component
560 is used (0.90 ± 0.23 mm/yr). These results confirm our previous conclusions based on the
561 residual trend maps.

562 In Table 3, the mean North Atlantic residual trends presented in Figure 9, 12 and 13 are
563 quantified.

564

565 *Table 3. Mean North Atlantic residual trends (mm/yr) for different products of the sea level*
566 *budget.*

Trends(mm/yr)	GRACE manometric (GMSL trend added)	GRACE manometric (GMSL trend removed)	CIGAR manometric (GMSL trend removed)
SIO (0-2000m) +Deep Ocean	1.89 ± 0.21	1.53 ± 0.21	0.88 ± 0.20
CIGAR (Full depth)	1.51 ± 0.23	0.90 ± 0.23	0.24 ± 0.22

567

568 **4 Discussion**

569 In this study, we have revisited the sea level budget of the North Atlantic over the 2004-2022
570 period, using a variety of different data sets. The objective was to further investigate the results
571 from Bouih et al. (2025) who reported non-closure of the sea level budget in the North Atlantic
572 over the same time span, and to identify which components of the budget (or which missing
573 component) are responsible.

574 The main results of our study can be summarized as follows:



- 575 (1) By comparing the SIO-based steric sea level with “Altimetry minus manometric sea
576 level” in two cases (GRACE and CIGAR-based manometric component) over the North
577 Atlantic, the use of CIGAR manometric sea level provides higher correlation than when
578 using GRACE. This comparison indicates potential errors in the GRACE and GRACE-
579 FO data, particularly in the eastern region of the North Atlantic basin where the
580 manometric component is strongly negative. The cause is so far unknown but possibly
581 related to the correction applied to GRACE data, e.g., the geocenter or GIA corrections.
582 These needs dedicated investigation.
- 583 (2) As of 2012, a decreasing trend is observed in the SIO halosteric component which
584 suggests a physically real increase in salinity of the North Atlantic. Again, this needs
585 further investigation.
- 586 (3) Our study shows that the deep ocean (>2000 m of depth) contribution to the North
587 Atlantic sea level budget is not negligible and needs to be taken into account to obtain
588 better closure of the sea level budget in this region. Based on CIGAR, the additional
589 deep ocean steric contribution (above the global mean deep ocean contribution) to the
590 North Atlantic sea level budget amounts to 0.62 ± 0.04 mm/yr.
- 591 (4) Accounting for the deep ocean steric contribution reduces by a factor of 30% the
592 residuals of the North Atlantic sea level budget when using the GRACE manometric
593 component, and by a factor of two when using CIGAR for the manometric component
594 (and CIGAR full depth for the steric component). In the latter case, the mean residual
595 trend over the North Atlantic is <1mm/yr, i.e., of the same order of magnitude as the
596 regional trend error for altimetry gridded data according to Prandi et al. (2021). We can
597 thus conclude that the closure of the sea level budget holds within the data uncertainties
598 in this case.



599 (5) Our results also indicate that the main contribution to the mean North Atlantic residual
600 trend comes from errors on the regional components (whatever the products used for
601 the components) rather than from errors in the global mean trends.

602 (6) The North Atlantic sea level budget is closed within data uncertainties when using the
603 CIGAR reanalysis for both the manometric and steric components.

604 (7) Our study also shows that the sea level budget of all other oceans (North Atlantic
605 excluded) is almost closed when accounting for the deep ocean steric contribution based
606 on the CIGAR ocean reanalysis

607 These new findings represent a step further towards better understanding of the present-day sea
608 level budget in the North Atlantic region. Those investigations also support the need to better
609 observe the deep ocean especially in the North Atlantic Ocean which is one of the objectives
610 of the One Argo Project (Thierry et al., 2025). Nevertheless, some issues still merit deeper
611 investigation. We can quote the followings, among others: Why GRACE manometric data give
612 less good results in the North Atlantic than the CIGAR-based manometric sea level? Which
613 inaccurate correction applied to GRACE is involved? Is it related to the GIA or the geocenter
614 corrections applied to GRACE? What causes the slight salinity increase observed in the North
615 Atlantic (full depth) with SIO data? Can we explain the physical process causing the reported
616 CIGAR-based positive deep ocean steric sea level? What is the impact on the CIGAR steric
617 component estimates of the use of EN4 (with no salinity drift correction applied) in the
618 assimilation procedure? What is the source of the (small) remaining residual trend of the North
619 Atlantic sea level budget (after accounting for the deep ocean)? Clearly, future studies should
620 be devoted to try answering these puzzling questions.

621



622 **Author contributions**

623 AC, WL and ZS designed the study. All analyses have been performed by ZS. ZS and AC
624 wrote a first version of the manuscript. All co-authors contributed to the discussion of the
625 results, editing and final writing of the manuscript.

626

627 **Competing interests**

628 The contact author has declared that none of the authors has any competing interests.

629

630 **Acknowledgements**

631 Zhe Song is supported by China Scholarship Council. This study is a contribution to the
632 ongoing ESA (European Space Agency) CCI (Climate Change Initiative) project entitled ‘Sea
633 level budget closure CCI+ (SLBC_CCI+)’. This work is a contribution to the GREAT project
634 funded by CNES through the Ocean Surface Topography Science Team (OSTST).

635



636 **References**

- 637 Adhikari, S., Ivins, E. R., Frederikse, T., Landerer, F. W., and Caron, L.: Sea-level fingerprints
638 emergent from GRACE mission data, *Earth System Science Data*, 11, 629–646,
639 <https://doi.org/10.5194/essd-11-629-2019>, 2019.
- 640 Barnoud, A., Pfeffer, J., Guérou, A., Frery, M., Siméon, M., Cazenave, A., Chen, J., Llovel,
641 W., Thierry, V., Legeais, J., and Ablain, M.: Contributions of Altimetry and Argo to Non-
642 Closure of the Global Mean Sea Level Budget Since 2016, *Geophysical Research Letters*, 48,
643 <https://doi.org/10.1029/2021gl092824>, 2021.
- 644 Bouih, M., Barnoud, A., Yang, C., Storto, A., Blazquez, A., Llovel, W., Fraudeau, R., and
645 Cazenave, A.: Regional sea level trend budget over 2004–2022, *Ocean Sci.*, 21, 1425–1440,
646 <https://doi.org/10.5194/os-21-1425-2025>, 2025.
- 647 Brown, S., Willis, J., and Fournier, S.: Jason-3 Wet Path Delay Correction,
648 <https://doi.org/10.5067/J3L2G-PDCOR>, 2023.
- 649 Camargo, C. M. L., Riva, R. E. M., Hermans, T. H. J., Schütt, E. M., Marcos, M., Hernandez-
650 Carrasco, I., and Slangen, A. B. A.: Regionalizing the sea-level budget with machine learning
651 techniques, *Ocean Science*, 19, 17–41, <https://doi.org/10.5194/os-19-17-2023>, 2023.
- 652 Chen, J., Tapley, B., Seo, K., Wilson, C., and Ries, J.: Improved Quantification of Global Mean
653 Ocean Mass Change Using GRACE Satellite Gravimetry Measurements, *Geophys. Res. Lett.*,
654 46, 13984–13991, <https://doi.org/10.1029/2019GL085519>, 2019.
- 655 Chen, J., Tapley, B., Wilson, C., Cazenave, A., Seo, K.-W., and Kim, J.-S.: Global Ocean Mass
656 Change From GRACE and GRACE Follow-On and Altimeter and Argo Measurements,
657 *Geophysical Research Letters*, 47, e2020GL090656, <https://doi.org/10.1029/2020GL090656>,
658 2020.
- 659 Cheng, L., Zhu, J., Cowley, R., Boyer, T., and Wijffels, S.: Time, Probe Type, and Temperature
660 Variable Bias Corrections to Historical Expendable Bathythermograph Observations, *Journal*



661 of Atmospheric and Oceanic Technology, 31, 1793–1825, <https://doi.org/10.1175/JTECH-D->
662 13-00197.1, 2014.

663 Dieng, H. B., Cazenave, A., Meyssignac, B., and Ablain, M.: New estimate of the current rate
664 of sea level rise from a sea level budget approach, *Geophysical Research Letters*, 44, 3744–
665 3751, <https://doi.org/10.1002/2017GL073308>, 2017.

666 Dobslaw, H., Bergmann-Wolf, I., Dill, R., Poropat, L., Thomas, M., Dahle, C., Esselborn, S.,
667 König, R., and Flechtner, F.: A new high-resolution model of non-tidal atmosphere and ocean
668 mass variability for de-aliasing of satellite gravity observations: AOD1B RL06, *Geophysical*
669 *Journal International*, 211, 263–269, <https://doi.org/10.1093/gji/ggx302>, 2017.

670 Flechtner, F., Dobslaw, H., and Fagiolini, E.: GRACE AOD1B product description document
671 for product release 05, 2014.

672 Frederikse, T., Riva, R., Kleinherenbrink, M., Wada, Y., van den Broeke, M., and Marzeion,
673 B.: Closing the sea level budget on a regional scale: Trends and variability on the Northwestern
674 European continental shelf, *Geophysical Research Letters*, 43, 10,864–10,872,
675 <https://doi.org/10.1002/2016GL070750>, 2016.

676 Gregory, J. M., Griffies, S. M., Hughes, C. W., Lowe, J. A., Church, J. A., Fukimori, I., Gomez,
677 N., Kopp, R. E., Landerer, F., Cozannet, G. L., Ponte, R. M., Stammer, D., Tamisiea, M. E.,
678 and van de Wal, R. S. W.: Concepts and Terminology for Sea Level: Mean, Variability and
679 Change, Both Local and Global, *Surv Geophys*, 40, 1251–1289,
680 <https://doi.org/10.1007/s10712-019-09525-z>, 2019.

681 Hamlington, B. D., Gardner, A. S., Ivins, E., Lenaerts, J. T. M., Reager, J. T., Trossman, D. S.,
682 Zaron, E. D., Adhikari, S., Arendt, A., Aschwanden, A., Beckley, B. D., Bekaert, D. P. S.,
683 Blewitt, G., Caron, L., Chambers, D. P., Chandanpurkar, H. A., Christianson, K., Csatho, B.,
684 Cullather, R. I., DeConto, R. M., Fasullo, J. T., Frederikse, T., Freymueller, J. T., Gilford, D.
685 M., Giroto, M., Hammond, W. C., Hock, R., Holschuh, N., Kopp, R. E., Landerer, F., Larour,
686 E., Menemenlis, D., Merrifield, M., Mitrovica, J. X., Nerem, R. S., Nias, I. J., Nieves, V.,



687 Nowicki, S., Pangaluru, K., Piecuch, C. G., Ray, R. D., Rounce, D. R., Schlegel, N.-J.,
688 Seroussi, H., Shirzaei, M., Sweet, W. V., Velicogna, I., Vinogradova, N., Wahl, T., Wiese, D.
689 N., and Willis, M. J.: Understanding of Contemporary Regional Sea-Level Change and the
690 Implications for the Future, *Reviews of Geophysics*, 58, e2019RG000672,
691 <https://doi.org/10.1029/2019RG000672>, 2020.

692 Horwath, M., Gutknecht, B. D., Cazenave, A., Palanisamy, H. K., Marti, F., Marzeion, B.,
693 Paul, F., Le Bris, R., Hogg, A. E., Otsuka, I., Shepherd, A., Döll, P., Cáceres, D., Müller
694 Schmied, H., Johannessen, J. A., Nilsen, J. E. Ø., Raj, R. P., Forsberg, R., Sandberg Sørensen,
695 L., Barletta, V. R., Simonsen, S. B., Knudsen, P., Andersen, O. B., Rannald, H., Rose, S. K.,
696 Merchant, C. J., Macintosh, C. R., von Schuckmann, K., Novotny, K., Groh, A., Restano, M.,
697 and Benveniste, J.: Global sea-level budget and ocean-mass budget, with a focus on advanced
698 data products and uncertainty characterisation, *Earth System Science Data*, 14, 411–447,
699 <https://doi.org/10.5194/essd-14-411-2022>, 2022.

700 Liu, C., Liang, X., Chambers, D., and Ponte, R.: Global Patterns of Spatial and Temporal
701 Variability in Salinity from Multiple Gridded Argo Products, *Journal of Climate*,
702 <https://doi.org/10.1175/JCLI-D-20-0053.1>, 2020.

703 Llovel, W. and Hochet, A.: Salinity Contribution to Regional Sea Level Trends in the Tropical
704 Southwestern Pacific Ocean Over 2014–2023, *Geophysical Research Letters*, 52,
705 e2025GL116115, <https://doi.org/10.1029/2025GL116115>, 2025.

706 Llovel, W., Balem, K., Tajouri, S., and Hochet, A.: Cause of Substantial Global Mean Sea
707 Level Rise Over 2014–2016, *Geophysical Research Letters*, 50, e2023GL104709,
708 <https://doi.org/10.1029/2023GL104709>, 2023.

709 McDougall, T. J., Barker, P. M., Marine, CSIRO., and Research, A.: Getting started with
710 TEOS-10 and the gibbs seawater (GSW) oceanographic toolbox, Trevor J. McDougall, 2011.



- 711 Mu, D., Church, J. A., King, M., Ludwigsen, C. B., and Xu, T.: Contrasting Discrepancy in the
712 Sea Level Budget Between the North and South Atlantic Ocean Since 2016, *Earth and Space*
713 *Science*, 11, e2023EA003133, <https://doi.org/10.1029/2023EA003133>, 2024.
- 714 Nerem, R. S., Beckley, B. D., Fasullo, J. T., Hamlington, B. D., Masters, D., and Mitchum, G.
715 T.: Climate-change–driven accelerated sea-level rise detected in the altimeter era, *Proceedings*
716 *of the National Academy of Sciences*, 115, 2022–2025,
717 <https://doi.org/10.1073/pnas.1717312115>, 2018.
- 718 Pardaens, A. K., Gregory, J. M., and Lowe, J. A.: A model study of factors influencing
719 projected changes in regional sea level over the twenty-first century, *Clim Dyn*, 36, 2015–2033,
720 <https://doi.org/10.1007/s00382-009-0738-x>, 2011.
- 721 Peltier, W. R., Argus, D. F., and Drummond, R.: Comment on “An Assessment of the ICE-
722 6G_C (VM5a) Glacial Isostatic Adjustment Model” by Purcell et al.: The ICE-6G_C (VM5a)
723 GIA model, *J. Geophys. Res. Solid Earth*, 123, 2019–2028,
724 <https://doi.org/10.1002/2016JB013844>, 2018.
- 725 Ponte, R. M., Sun, Q., Liu, C., and Liang, X.: How Salty Is the Global Ocean: Weighing It All
726 or Tasting It a Sip at a Time?, *Geophysical Research Letters*, 48, e2021GL092935,
727 <https://doi.org/10.1029/2021GL092935>, 2021.
- 728 Roemmich, D. and Gilson, J.: The 2004–2008 mean and annual cycle of temperature, salinity,
729 and steric height in the global ocean from the Argo Program, *Progress in Oceanography*, 82,
730 81–100, <https://doi.org/10.1016/j.pocean.2009.03.004>, 2009.
- 731 Royston, S., Dutt Vishwakarma, B., Westaway, R., Rougier, J., Sha, Z., and Bamber, J.: Can
732 We Resolve the Basin-Scale Sea Level Trend Budget From GRACE Ocean Mass?, *Journal of*
733 *Geophysical Research: Oceans*, 125, e2019JC015535, <https://doi.org/10.1029/2019JC015535>,
734 2020.



735 Storto, A. and Yang, C.: Acceleration of the ocean warming from 1961 to 2022 unveiled by
736 large-ensemble reanalyses, *Nat Commun*, 15, 545, [https://doi.org/10.1038/s41467-024-44749-](https://doi.org/10.1038/s41467-024-44749-7)
737 7, 2024.

738 Sun, Y., Riva, R., and Ditmar, P.: Optimizing estimates of annual variations and trends in
739 geocenter motion and J_2 from a combination of GRACE data and geophysical models, *J.*
740 *Geophys. Res. Solid Earth*, 121, 8352–8370, <https://doi.org/10.1002/2016JB013073>, 2016.

741 Tapley, B., Watkins, M., Flechtner, F., Reigber, C., Bettadpur, S., Rodell, M., Sasgen, I.,
742 Famiglietti, J., Landerer, F., Chambers, D., Reager, J., Gardner, A., Save, H., Ivins, E.,
743 Swenson, S., Boening, C., Dahle, C., Wiese, D., Dobslaw, H., and Velicogna, I.: Contributions
744 of GRACE to understanding climate change, *Nature Climate Change*, 5,
745 <https://doi.org/10.1038/s41558-019-0456-2>, 2019.

746 Thierry, V., Claustre, H., Pasqueron De Fommervault, O., Zilberman, N., Johnson, K. S., King,
747 B. A., Wijffels, S. E., Bhaskar, U. T. V. S., Balmaseda, M. A., Belbeoch, M., Bollard, M.,
748 Boutin, J., Boyd, P., Cancouët, R., Chai, F., Ciavatta, S., Crane, R., Cravatte, S., Dall’Olmo,
749 G., Desbruyères, D., Durack, P. J., Fassbender, A. J., Fennel, K., Fujii, Y., Gasparin, F.,
750 González-Santana, A., Gourcuff, C., Gray, A., Hewitt, H. T., Jayne, S. R., Johnson, G. C.,
751 Kolodziejczyk, N., Le Boyer, A., Le Traon, P.-Y., Llovel, W., Lozier, M. S., Lyman, J. M.,
752 McDonagh, E. L., Martin, A. P., Meyssignac, B., Mogensén, K. S., Morris, T., Oke, P. R.,
753 Smith, W. O., Owens, B., Poffa, N., Post, J., Roemmich, D., Rykaczewski, R. R.,
754 Sathyendranath, S., Scanderbeg, M., Scheurle, C., Schofield, O., Von Schuckmann, K.,
755 Scourse, J., Sprintall, J., Suga, T., Tonani, M., Van Wijk, E., Xing, X., and Zuo, H.: Advancing
756 ocean monitoring and knowledge for societal benefit: the urgency to expand Argo to OneArgo
757 by 2030, *Front. Mar. Sci.*, 12, 1593904, <https://doi.org/10.3389/fmars.2025.1593904>, 2025.

758 Wang, C., Dong, S., and Munoz, E.: Seawater density variations in the North Atlantic and the
759 Atlantic meridional overturning circulation, *Clim Dyn*, 34, 953–968,
760 <https://doi.org/10.1007/s00382-009-0560-5>, 2010.



761 WCRP: Global sea-level budget 1993–present, *Earth System Science Data*, 10, 1551–1590,
762 <https://doi.org/10.5194/essd-10-1551-2018>, 2018.

763 Wong, A. P. S., Gilson, J., and Cabanes, C.: Argo salinity: bias and uncertainty evaluation,
764 *Earth System Science Data*, 15, 383–393, <https://doi.org/10.5194/essd-15-383-2023>, 2023.

765 Wunsch, C., Ponte, R. M., and Heimbach, P.: Decadal Trends in Sea Level Patterns: 1993–
766 2004, *Journal of Climate*, 20, 5889–5911, <https://doi.org/10.1175/2007JCLI1840.1>, 2007.

767 Zuo, H., Balmaseda, M. A., Tietsche, S., Mogensen, K., and Mayer, M.: The ECMWF
768 operational ensemble reanalysis–analysis system for ocean and sea ice: a description of the
769 system and assessment, *Ocean Science*, 15, 779–808, <https://doi.org/10.5194/os-15-779-2019>,
770 2019.

771

772

773